TCP Reno and queue management: local stability and Hopf bifurcation analysis

A Project Report

submitted by

ARCHITH MOHAN

(EE09B007)

in partial fulfilment of the requirements
for the award of the degree of

BACHELOR OF TECHNOLOGY
in
ELECTRICAL ENGINEERING

DEPARTMENT OF ELECTRICAL ENGINEERING
INDIAN INSTITUTE OF TECHNOLOGY, MADRAS.

MAY 2013

PROJECT CERTIFICATE

This is to certify that the project titled **TCP Reno and queue management: local stability and Hopf bifurcation analysis**, submitted by **Archith Mohan (EE09B007)**, to the Indian Institute of Technology, Madras, for the award of the degree of **Bachelor of Technology**, is a bona fide record of the project work done by him under my supervision. The contents of this report, in full or in parts, have not been submitted to any other Institute or University for the award of any degree or diploma.

Dr. G. Raina
Project Guide
Assistant Professor
Dept. of Electrical Engineering
IIT Madras, Chennai 600 036

Place: Chennai

Date:

ACKNOWLEDGEMENTS

I thank God for blessing me with the health and strength required to complete this research project.

Many thanks is owed to Dr. Gaurav Raina for his support, guidance and motivation during the past one year. He has been much more than an advisor and I thank him for taking an earnest interest in my career.

I extend my appreciation to Mr. Shankar Raman for his help with the NS2 Simulations and NetFPGA experiments.

My parents are my pillars of strength. I would like to thank them for their unwavering financial and emotional support throughout my degree.

ABSTRACT

KEYWORDS: TCP Reno; NetFPGA; queue management; stability; Hopf bifurcation; packet-level simulations; NetFPGA experiments.

Using a combination of analysis, numerical computations and packet-level simulations, we study the dynamics of TCP Reno which is a standardised transport protocol for the Internet. We systematically study local stability and the local Hopf bifurcation properties, of a fluid model for TCP Reno coupled with four queue management schemes in routers. Models for the widely deployed Drop-Tail queue policy, over two different router buffer sizing regimes are considered. We also consider a model for a threshold based queue policy and a Drop-Tail queue policy with bursty flows. We explicitly show that variations in parameters like the buffer size can produce Hopf induced limit cycles in the queue size. It is practically important, and theoretically demanding, to characterise the existence, uniqueness and stability of the bifurcating periodic solutions. Using the theory of normal forms and the center manifold theorem, we establish that the Hopf bifurcation is indeed supercritical. Packet-level simulations and NetFPGA emulations for the Drop-Tail queue policy corroborate our theoretical analysis. Some design considerations to ensure stability of queue sizes for high-speed communication networks are outlined.

TABLE OF CONTENTS

LIST OF TABLES

LIST OF FIGURES

ABBREVIATIONS

AQM	Active Queue Management
RED	Random Early Detection
RTT	Round-trip Time
TCP	Transmission Control Protocol

CHAPTER 1

Introduction

1.1 Motivation

The Transmission Control Protocol (TCP) plays a critical role in providing end-to-end performance for applications that run over the Internet. Traditionally, the analysis of transport protocols has been performed using discrete-event packet-level simulations (1). Another approach for performance analysis is to construct fluid models for the underlying packet based system, and then use the stability properties of the model to guide design and performance considerations. Fluid based analysis of transport protocols are useful as they allow the study of network dynamics in a scalable and computationally inexpensive way. For motivation on the model for TCP Reno, see (9; 11; 12).

With increasing traffic in the Internet, congestion avoidance and control assumes significance. The key elements of congestion control are the congestion avoidance algorithms embedded in transport protocols. When queues are overloaded, they drop packets. Such dropped packets serve to provide indications of congestion, in the network, to end-systems. Thus queue management policies and the size of router buffers also play an integral part in network performance. For early work on router buffer sizes see (12; 15), and for some queuing models, see (7; 12). We note that there is still no agreement on the optimal design choices for transport protocols, queue policies, or router buffer sizes.

One way to approach the problem is to study the dynamics of existing congestion control systems using a combination of analysis, numerical computations and packet-level simulations. Once the short-comings are exposed, the ways to address them can be explored.

1.2 Problem Description

In this thesis, we focus on the standardized TCP Reno and study it in combination with four different queue management models. The models for queue management we study are a Drop-Tail queue policy for smooth flows, with an intermediate and a small buffer regime, a Drop-Tail queue policy for bursty flows with a small buffer regime, and a threshold based queue management policy. Using a combination of queuing, control, and bifurcation theory supplemented with numerical and packet-level simulations, we analyse the underlying models for their local stability and Hopf bifurcation properties.

We also study the system by emulating with NetFPGA (4), an open networking platform accelerator that enables researchers and instructors to build working prototypes of high-speed, hardware-accelerated networking systems. NetFPGA based routers have often been deployed in the Internet for experimental purposes and have been shown to be more precise than software based traffic generators (2). Other than transmitting experimental TCP Reno traffic, NetFPGA also supports traffic from routing protocols thereby providing a more realistic scenario for conducting experiments. The NetFPGA emulation further supplements our local stability and Hopf bifurcation analysis.

1.3 Contributions

In this thesis, we first proceed to outline sufficient conditions for local stability, and characterise the necessary and sufficient conditions. The associated stability charts for these conditions inform us that minor variations in parameters at the router-level algorithms can make the system enter a locally unstable state. We show that this transition occurs via a Hopf bifurcation as parameters like buffer size are varied. A practical manifestation of a Hopf bifurcation, in communication networks, is the formation of limit cycles in the queue size. Employing the theory of normal forms and the cen-

ter manifold theorem, we show that the Hopf bifurcation is supercritical. Thus we are able to theoretically characterise the existence, uniqueness and stability of the bifurcating periodic solutions. The existence of the theoretically predicted stable limit cycles are validated with packet-level simulations using Network Simulator (NS2) (16) and emulation using NetFPGA.

1.4 Organisation

The rest of this thesis is organised as follows. In Chapter 2, we present a nonlinear fluid model for TCP Reno and we outline the four queue management strategies. Chapter 3 contains the local stability analysis and some robustness considerations for the system. In Chapter 4, we confirm that the local Hopf bifurcation is supercritical. In Chapter 5, we provide evidence of limit cycles in the queue size dynamics using packet-level simulations and NetFPGA emulation. In Chapter 6, we summarize our contributions. To support the results in Chapter 4, a complete characterization of local Hopf bifurcation analysis is presented in a self contained Appendix.

CHAPTER 2

Models

2.1 Non-linear fluid model for TCP Reno

Consider a collection of N TCP flows with common round-trip time τ, subject to a common packet loss probability $p(x(t))$. The average window size of all N flows at a time t is given by $w(t)$, measured in packets, so that the average sending rate becomes $x(t) = w(t)/\tau$. For TCP Reno, the window $w(t)$ increases by 1 every τ, and decreases by $w(t)/2$ in case packet loss is detected due to congestion. The form of $p(t)$ determines the queue management policy adopted in the network. The fluid model for the congestion avoidance phase of TCP Reno is given by

$$\frac{dw(t)}{dt} = \frac{1}{\tau} - \frac{w(t)}{2}\Big(x(t-\tau)p(t-\tau)\Big). \tag{2.1}$$

There are arguments in favour of such a non-linear model for TCP Reno in (11). In the next section, we describe fluid models for the different queue management policies under consideration.

2.2 Models for Queue Management

We consider four models for packet drop policy. These are: small buffer Drop-Tail for smooth and bursty flows, intermediate buffer Drop-Tail and a threshold based drop policy. Let the drop probability be given by $p(x)$. Then the four models can be described as follows:

1) It is suggested that for a large number of flows, the blocking probability of a M/M/1 queue is a reasonable model for the packet loss incurred by a small buffered

router that implements the Drop-Tail mechanism (11; 12). A packet is dropped if it arrives at the queue to find at least B packets already present. Thus, the fluid-level representation for the queue may be given by

$$p(x) = \left(\frac{x}{C}\right)^B, \tag{2.2}$$

where C is the link capacity and B is the buffer size.

2) In a Drop-Tail scheme, data packets that arrive later get dropped when a buffer overflows in the router. The loss probability of such a queue may be modelled as a $M/M/1/B$ queue, where B is the buffer size. For such a system we have,

$$p(x) = \frac{(1-\rho)\rho^B}{1-\rho^{B+1}},$$

where $\rho = x/C$. If the arrival rate x, capacity C, and the buffer size B are scaled by a factor β, as in many-flows large-deviation scaling, then by letting $\beta \to \infty$ we get,

$$\lim_{\beta\to\infty} \frac{(1-\rho)\rho^{B\beta}}{1-\rho^{B\beta+1}} = \left(\frac{x-C}{x}\right)^+. \tag{2.3}$$

Note that in a fluid model, this denotes the fraction of fluid lost when the arrival is greater than the capacity. This models an intermediate buffer Drop-Tail queue management scheme (8; 12).

3) For the purpose of defining the threshold algorithm for queue management, we assume the workload arriving at the receiver over a time-period τ as having a Gaussian distribution, with a mean $x\tau$ and variance $x\tau\sigma^2$. If the workload exceeds a threshold level B, then the incoming packet is dropped. The expression for the the queue management strategy is obtained from (7), and is given by

$$p(x) = \exp\left(\frac{-2B(C-x)}{x\sigma^2}\right). \tag{2.4}$$

4) For packets arriving in bursts, we consider a batch Poisson traffic model. In a

queue fed by a Poisson process of rate x/n, each Poisson arrival represents the arrival of a burst of n packets. Then a simple fluid model for the queue could be

$$p(x) = \left(\frac{x}{C}\right)^{B/n}. \tag{2.5}$$

For more motivation on the model, see (12; 13).

The expressions for the drop probabilities, (2.2), (2.3), (2.4), and (2.5) are substituted into the non-linear model for TCP Reno obtained from (2.1). On substituting, we obtain four TCP Reno-queue management models, referred to in the rest of the thesis as Models I, II, III and IV.

CHAPTER 3

Local Stability

In this chapter, we proceed to determine the steady state solution for the non-linear model for TCP Reno for a general $p(x)$. We then linearise the model about the state steady state point and determine the necessary and sufficient conditions for local stability. We also construct relevant stability charts.

Equation (2.1) can be written as

$$\frac{dx(t)}{dt} = \frac{1}{\tau^2} - \frac{x(t)}{2}\Big[x(t-\tau)p(x(t-\tau))\Big], \tag{3.1}$$

since the packet drop probability is a function of the rate x and $w(t) = x(t)\tau$.

The equilibrium for equation (3.1) occurs at $x_0 = \frac{1}{\tau}\sqrt{\frac{2}{p}}$. The equilibrium is unique as sending rates have to be non-negative. On linearising about the equilibrium, we get

$$\begin{aligned}\frac{dx(t)}{dt} &= \frac{-x_0}{2}p(x_0)(x(t)-x_0) \\ &\quad -\frac{x_0}{2}\Big(x_0p'(x_0) + p(x_0)(x(t-\tau)-x_0)\Big).\end{aligned} \tag{3.2}$$

Substituting $u(t) = x(t) - x_0$ and $u(t-\tau) = x(t-\tau) - x_0$ in equation (3.2), we get the linearised delay-differential equation in the standard form given by

$$\frac{du(t)}{dt} = -au(t) - bu(t-\tau).$$

Table 3.1: Necessary and sufficient conditions for local stability for Models I, II, III and IV

	Necessary and sufficient condition for local stability
I	$\frac{1}{w_s}\sqrt{B(B+2)} < \cos^{-1}\left(-\frac{1}{B+1}\right)$
II	$\frac{C\tau}{2}\sqrt{\frac{2w_s}{C\tau}-1} < \cos^{-1}\left(-\frac{2}{w_s^2}\right)$
III	$\frac{w_s}{2}p(w_s)\sqrt{\frac{2BC\tau}{\sigma^2 w_s}} < \cos^{-1}\left(-\frac{\sigma^2 w_s}{\sigma^2 w_s + 2BC\tau}\right)$
IV	$\frac{1}{w_s}\sqrt{(B/n)(B/n+2)} < \cos^{-1}\left(-\frac{1}{B/n+1}\right)$

For $a \geq 0$, $b > 0$, $b > a$ and $\tau > 0$, it can be shown that (10)

$$b\tau < \frac{\pi}{2}, \tag{3.3}$$

is a sufficient condition for local stability. The necessary and sufficient condition for local stability is given by

$$\tau\sqrt{b^2 - a^2} < \cos^{-1}\left(-\frac{a}{b}\right). \tag{3.4}$$

Using results (3.3) and (3.4), we now find expressions for the necessary and sufficient condition for local stability. For Models I, II, III and IV, the necessary and sufficient conditions for local stability are presented in Table 3.1. From these we obtain sufficient conditions for stability which are presented in Table 3.2.

Figure 3.1 shows the stability charts for Models I, III and IV for link capacity $C = 140$ packets/second, $\sigma^2 = 3$ packets and $n = 10$. The stability charts clearly show that the system is stable only in the small buffer regime. Model II is always unstable except for small values of τ and link capacity C.

In the parameter space where the system is stable, it is possible to obtain a necessary and sufficient condition for the existence of overdamped solutions. Consider the

Table 3.2: Sufficient conditions for local stability for Models I, II, III and IV

	Sufficient condition for local stability
I	$\frac{B+1}{w_s} < \frac{\pi}{2}$
II	$w_s < \pi$
III	$w_s p(w_s)\left(1 + \frac{2BC\tau}{\sigma^2 w_s}\right) < \pi$
IV	$\frac{B/n+1}{w_s} < \frac{\pi}{2}$

characteristic equation of the system reproduced here:

$$\lambda + a + b\exp(-\lambda\tau) = 0. \tag{3.5}$$

Let $\lambda = \sigma + j\omega$. For an overdamped response, $\sigma < 0$ and $\omega = 0$. For $\lambda = \sigma$, we have

$$\sigma + a + b\exp(-\sigma\tau) = 0. \tag{3.6}$$

For the above characteristic equation to have solutions with $\sigma < 0$, the minima of $f(\sigma) = \sigma + a + b\exp(-\sigma\tau)$ must be less than zero. From this we get the necessary and sufficient condition for the existence of overdamped solutions as

$$b\tau < \exp(-a\tau - 1). \tag{3.7}$$

The necessary and sufficient conditions for the existence of over-damped solutions for Models I, II, III and IV have been compiled in Table 3.3. It is easy to see that

$$b\tau < \exp(-1), \tag{3.8}$$

is a necessary condition for the existence of over-damped solutions.

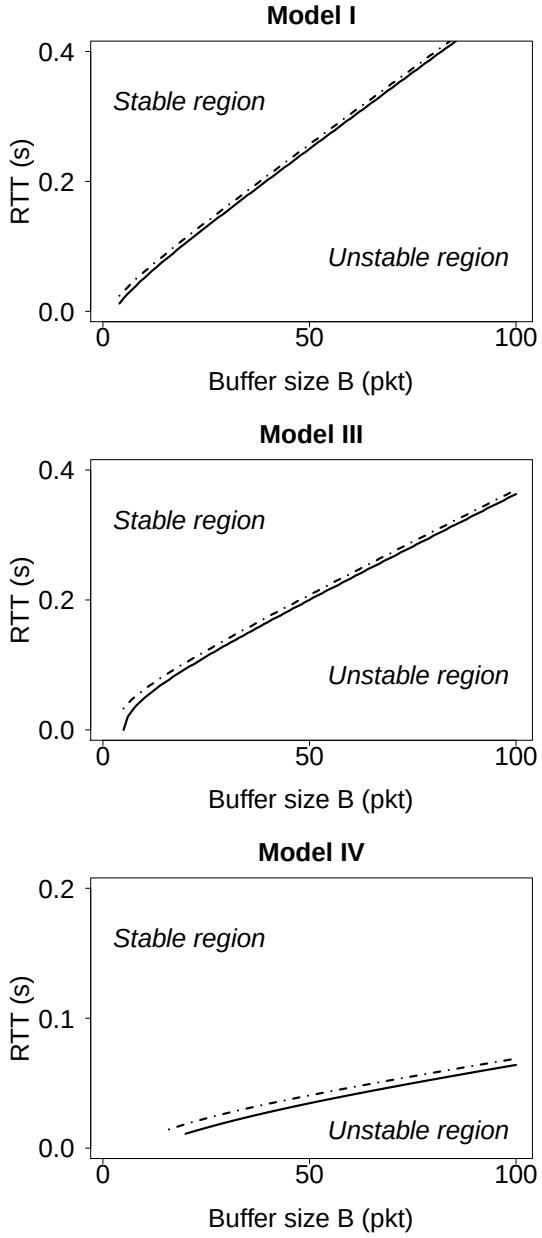

Figure 3.1: Stability charts for Models I, III and IV for link capacity $C = 140$ packets/second. The dashed line represents the boundary of the stable region in which the necessary and sufficient condition for stability given in Table 3.1 is satisfied. The solid line represents the boundary of the region in which sufficient condition for stability given in Table 3.2 holds true.

The results in this section show that in case of Models I, III and IV, using small buffers will ensure local stability. In the case of Model II, the equilibrium window size must be extremely small to ensure local stability.

Table 3.3: Necessary and sufficient conditions for the existence of overdamped solutions for Models I, II, III and IV

	Necessary and sufficient condition for the existence of over-damped solutions
I	$\frac{B+1}{w_s} < \exp\left(-\frac{1}{w_s} - 1\right)$
II	$\frac{w_s}{2} < \exp\left(-\frac{1}{w_s} - 1\right)$
III	$\frac{w_s}{2} p(w_s) \left(1 + \frac{2BC\tau}{\sigma^2 w_s}\right) < \exp\left(-\frac{1}{w_s} - 1\right)$
IV	$\frac{B/n+1}{w_s} < \exp\left(-\frac{1}{w_s} - 1\right)$

Robustness Considerations

The models considered in this thesis have uncertainty, both in the form of parameter variations and in the form of neglected dynamics. It is rather important that we quantify the variation in system stability and performance due to the before mentioned uncertainties. In this section, we use the Vinnicombe metric (14) to tackle the issue of parametric uncertainty in Model I. The approach can be extended to the other models.

Consider two transfer functions P_1 and P_2. Define $d(P_1, P_2)$ as

$$d\left(P_1, P_2\right) = \sup_{\omega} \frac{\left|P_1\left(i\omega\right) - P_2\left(i\omega\right)\right|}{\sqrt{\left(1 + \left|P_1\left(i\omega\right)\right|^2\right)\left(1 + \left|P_2\left(i\omega\right)\right|^2\right)}}, \tag{3.9}$$

where $d\left(P_1, P_2\right) \in \left[0, 1\right]$. Let C be the set of all pairs (P_1, P_2) such that the functions $f_1 = 1 + P_1(s)P_1(-s)$ and $f_2 = 1 + P_2(s)P_1(-s)$ have the same number of zeros in the right half-plane. The Vinnicombe metric is defined as

$$\delta_v(P_1, P_2) = \begin{cases} d(P_1, P_2), & if\ (P_1, P_2)\, \epsilon\, C \\ 1 & otherwise. \end{cases} \tag{3.10}$$

The Vinnicombe metric is a distance metric that serves as a proxy for similarity in stability properties and performance. In general, larger buffer sizes give higher link utilisation (12). Thus, it makes sense to operate the system along the edge of stability (given by the solid line in Figure 3.2). But then we run the risk of moving into the region of instability in the presence of parametric variations. One way of dealing with this is to operate at a new system operating point (given by the dashed line in Figure 3.2) at a distance given by a Vinnicombe metric of 0.1 from the edge of stability.

For Model I, we have assumed that there is no uncertainty in capacity C, buffer size B and the model. Uncertainty is present in the round-trip time. The loop transfer function for the linearised model is

$$P(s) = \frac{\left((B+1)/w_s\tau\right)\exp(-s\tau)}{s + (1/w_s\tau)}. \tag{3.11}$$

$P_1(s)$ is set up to correspond to the system operating at the edge of stability. The round-trip time is then varied in $P_2(s)$ to obtain the operating point which is at distance given by a Vinnicombe metric of 0.1.

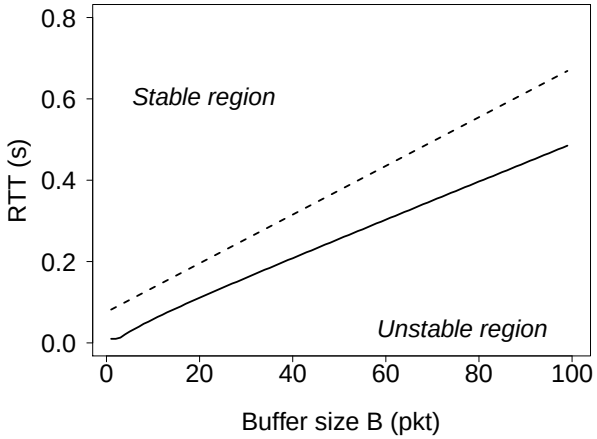

Figure 3.2: The solid line represents the edge of stability and the dashed line represents a collection of operating points at a distance given by a Vinnicombe metric of 0.1 from the edge of stability.

In the next chapter, we perform a Hopf bifurcation analysis of the system by forcing the system to transit into a region of instability using a system based parameter.

CHAPTER 4

Local Hopf Bifurcation

The non-linear model for TCP Reno is of the form

$$\frac{d}{dt}w(t) = \alpha f(w(t), w(t-\tau)). \tag{4.1}$$

Here α is a nondimensional exogenous parameter and $w(t)$ denotes window size at the time instant t.

The function $\alpha f(w(t), w(t-\tau))$ is dependent on the system parameters. It is possible to drive the system to the edge of stability using combinations of system parameter values. The system then undergoes a Hopf bifurcation if

$$\mathrm{Re}\left(\frac{d\lambda}{d\alpha}\right)_{\alpha=1} \neq 0, \tag{4.2}$$

the transversality condition of the Hopf spectrum, is satisfied. Here $\mathrm{Re}(.)$ represents the real part.

We single out buffer size B as our parameter of interest. For a particular value of link capacity C, we now construct the bifurcation diagrams for Models I, III and IV. For these models, we have a Hopf bifurcation for a particular value of buffer size B $(= B_c)$ for which the system transits from stability to instability. The transition occurs when the system moves away from a parameter space in which the conditions in Table 3.1 hold. The bifurcation point also needs to satisfy the transversality condition

$$\mathrm{Re}\left(\frac{d\lambda}{dB}\right)_{B=B_c} \neq 0. \tag{4.3}$$

The general expression for the transversality condition for Models I, II, III and IV is

given by

$$\left.\frac{db}{dB}\right|_{B=B_c} \frac{(a+b^2\tau)}{b\left(1+2a\tau+b^2\tau^2\right)} \neq 0. \tag{4.4}$$

Since $a \geq 0$, $b > 0$, $b > a$ and $\tau > 0$, we see from (4.4) that for the transversality condition to hold true, we just need

$$\left.\frac{db}{dB}\right|_{B=B_c} \neq 0. \tag{4.5}$$

For Models I, III and IV, (4.5) evaluates to a nonzero quantity. Thus the transversality condition (4.3) is satisfied.

The bifurcation diagrams, in Figure 4.1 are constructed for a link capacity C of 140 packets/second (with $\sigma^2 = 3$ packets for Model III). The figures highlight the link between system stability and the parameter B.

We now highlight the differences in the non-linear structure of Models I, II, III and IV, and perform an analytical characterization of the Hopf bifurcation.

Non-linear structure of Models I and II

Following the analysis in (6; 10), we preserve the non-linearity of (4.1) by retaining the quadratic and cubic terms in the Taylor series approximation about the equilibrium point. For convenience, we use $u(t) \equiv w(t) - w_s$, $x \equiv w(t)$ and $y \equiv w(t-\tau)$. Thus (4.1) transforms into

$$\begin{aligned}
\frac{d}{dt}u(t) &= \alpha\xi_x u(t) + \alpha\xi_y u(t-\tau) + \alpha\xi_{xx}u^2(t) \\
&\quad + \alpha\xi_{xy}u(t)u(t-\tau) + \alpha\xi_{yy}u^2(t-\tau) \\
&\quad + \alpha\xi_{xxx}u^3(t) + \alpha\xi_{xxy}u^2(t)u(t-\tau) \\
&\quad + \alpha\xi_{xyy}u(t)u^2(t-\tau) + \alpha\xi_{yyy}u^3(t-\tau) \\
&\quad + O(u^4),
\end{aligned} \tag{4.6}$$

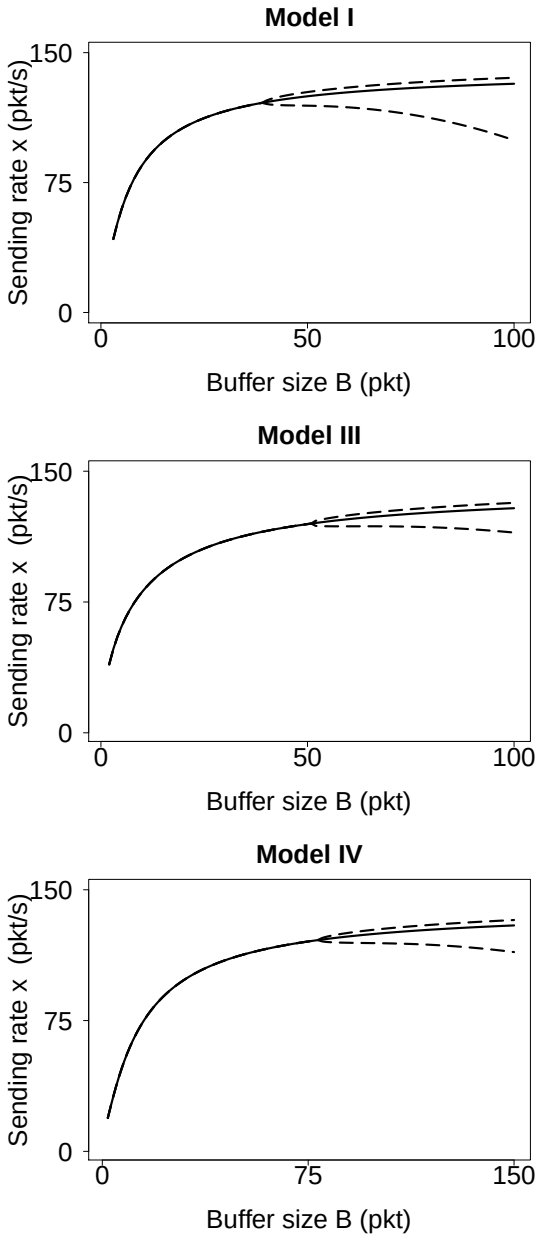

Figure 4.1: Bifurcation diagrams for Models I, III and IV showing the emergence of limit cycles as the buffer size increases beyond a certain threshold. Observe that system stability can be ensured only with small buffers and that the system performs better in the presence of bursty flows.

Table 4.1: Linear, quadratic and cubic terms of Models I and II

	Model I	Model II
ξ_x	$-\frac{w_s p(w_s)}{2\tau}$	$-\frac{w_s - C\tau}{2\tau}$
ξ_y	$-\frac{w_s p(w_s)}{2\tau}(B+1)$	$-\frac{w_s}{2\tau}$
ξ_{xx}	0	0
ξ_{yy}	$-\frac{p(w_s)}{2}(B+1)$	0
ξ_{xy}	$-\frac{p(w_s)}{4}B(B+1)$	$-\frac{1}{2}$
ξ_{xxx}	0	0
ξ_{xxy}	0	0
ξ_{xyy}	$-\frac{p(w_s)\tau}{4w_s}B(B+1)$	0
ξ_{yyy}	$-\frac{p(w_s)\tau}{12w_s}B(B-1)(B+1)$	0

where

$$\xi_{x^i y^j} = \frac{1}{(i+j)!}\frac{\partial^{i+j}}{\partial x^i \partial y^j} f \Big|_{x=x_s, y=y_s}. \tag{4.7}$$

In Table 4.1 we have listed out the linear, cubic and quadratic terms (4.7) for Models I and II, to highlight the differences in their non-linear structure. The linear and higher order terms for Models III and IV can be calculated using (4.7) but are not shown. The $\xi_{x^i y^j}$'s are used to analytically characterise the Hopf bifurcation. The complete local Hopf bifurcation analysis is shown in the Appendix.

In the Appendix, we describe two quantities, μ_2 and β_2, used to analytically char-

Table 4.2: Period of Hopf Bifurcations for Models I, III and IV

	Period of Hopf Bifurcations
I	$\frac{2\pi\tau}{\cos^{-1}\left(-\frac{1}{B+1}\right)}$
III	$\frac{2\pi\tau}{\cos^{-1}\left(-\frac{\sigma^2 w_s}{\sigma^2 w_s + 2BC\tau}\right)}$
IV	$\frac{2\pi\tau}{\cos^{-1}\left(-\frac{1}{B/n+1}\right)}$

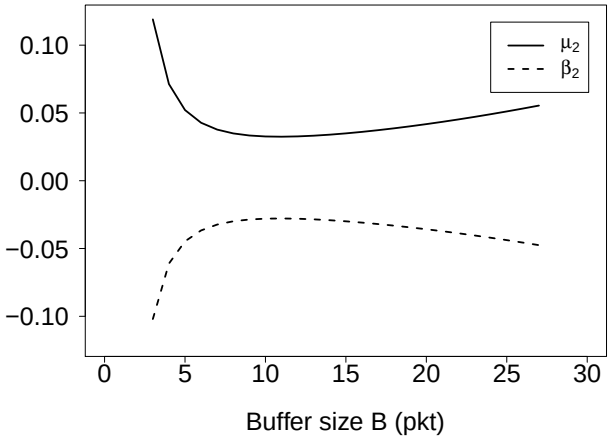

Figure 4.2: Variation of μ_2 and β_2 with buffer size for Model I for a large bandwidth-delay product. Note that $\mu_2 > 0$ and $\beta_2 < 0$ for all values of buffer size. Thus, the Hopf bifurcation is always supercritical. See the Appendix for all definitions and associated analysis.

acterise the Hopf bifurcation; see A.8. Figure 4.2 is representative of the variation of μ_2 and β_2 with buffer size B for Models I, III and IV for a link capacity of C of 140 packets/second and $\tau = 200$ ms. From the figure, we see that $\mu_2 > 0$ and $\beta_2 < 0$ for all values of buffer size B. Hence, we conclude that the Hopf bifurcation is always stable and supercritical (see end of Appendix). In Table 4.2 we present the period of the (emergent) periodic orbits at the Hopf bifurcation point for Models I, III and IV. In the next chapter, we show using packet-level simulations that, in a practical scenario, limit cycles in the queue size manifest as synchronized flows.

CHAPTER 5

Packet-level simulations and NetFPGA emulation

The analyses conducted using the fluid model in the previous chapters indicate that the system will be unstable when operating with large buffer sizes. In this chapter we perform packet-level simulations using the network simulator-2 (NS2) (16) and TCP Reno under the Drop-Tail queue management strategy. We also perform emulation using a hardware NetFPGA (4) based router. Both are conducted on a single bottleneck topology. Our aim is to find out whether the results of the analysis will be valid for a real network during the congestion control phase of TCP Reno.

5.1 NS2 simulations

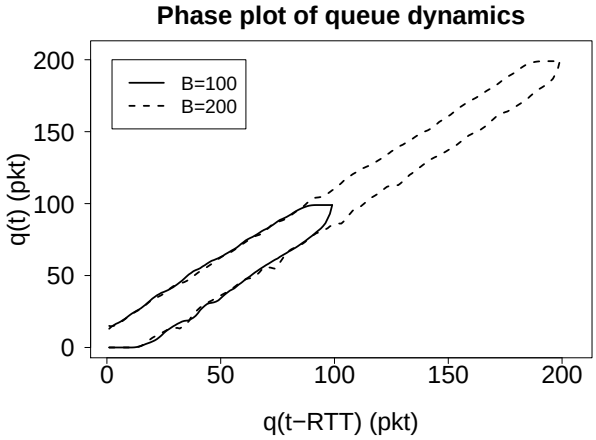

Figure 5.1: Phase diagram for queue size dynamics generated using data from packet-level simulations. Note the existence of limit cycles as buffer size varies. The time plot for the same is shown in the right hand side of Figure 5.2.

The following parameters were used for our simulations: buffer size = 10, 100 and 200 packets, with round-trip time $\tau = 200$ ms, bottleneck link capacity $C = 100$ Mbps,

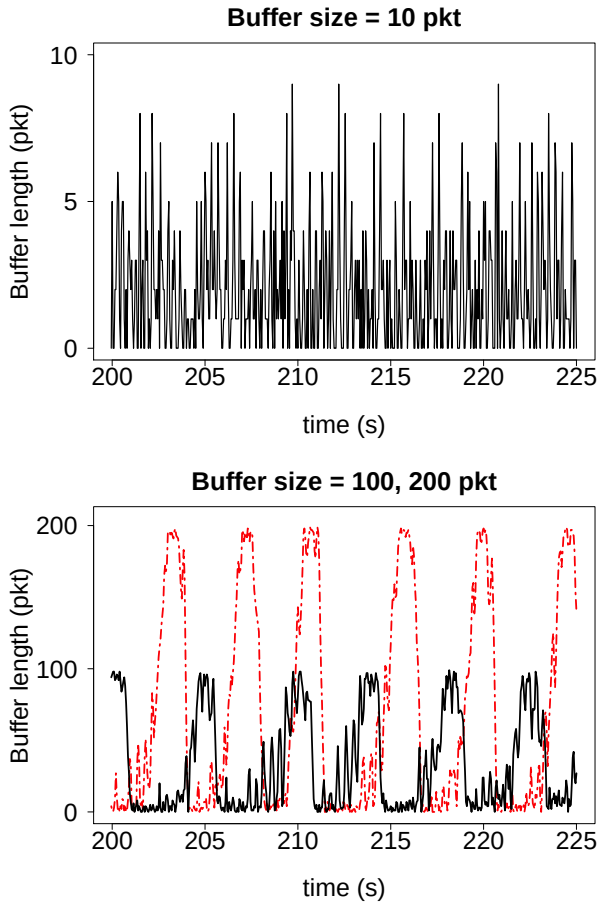

Figure 5.2: Packet-level simulations over a single bottleneck topology with link capacity = 100 Mbps, 60 flows with a τ of 200 ms and packet size of 1500 bytes. In the left, with small buffer sizes, we do not observe any limit cycles. On the right, as buffer sizes get larger, we witness the emergence of limit cycles [solid line represents 100 packets and dashed line represents 200 packets].

number of flows $N = 60$ and packet size = 1500 bytes. We observed the behaviour of the queue size in our simulations.

It has been shown in (7; 11), that even minor variations in buffer size can readily lead to instability. Figure 5.1 shows the phase diagram for the queue sizes. It is seen that the system does not converge and that with increasing τ the bounds for these cycles also increase. Figure 5.2 clearly shows that queue lengths are stochastically stable for a buffer size of 10 packets and that as the buffer size is increased to 100 and 200 packets, there is synchronization of flows. Such flow synchronization establishes the existence of stable limit cycles observed in Model I.

5.2 NetFPGA emulation

NetFPGA, developed at Stanford University, is a research and development platform to evaluate high speed networks (4). It consists of a Field Programmable Gate Array, which can handle switching, routing and data path processing. Gateware based on Verilog can be synthesized and logic mapped using Xilinx's ISE tools onto the FPGA. NetFPGA uses peripheral communication interconnect (PCI) expansion slot to communicate with the Linux operating system based host machine. The software interface for the NetFPGA consists of a Linux driver which allows user space software to communicate with the NetFPGA device and its registers. Other than collecting statistics about network traffic, these registers also act as a communication point between the host and the NetFPGA. The details about these registers are available in the NetFPGA documentation.

We used the NetFPGA platform's gateware and software based reference full line-rate internet router for our experiments. Our focus is confined to a single link topology, which is shown in Figure 5.3. We configured two computer systems that contained a 2.5 GHz Intel quad core processor and Intel dual port e1000 PCI express x4 NIC. A NetFPGA card was connected to Host 1. The parameters used in the experiments are outlined in Table 5.1.

Figure 5.3: Emulation setup uses 2 Linux machines running TCP client, server and a NetFPGA hardware router. The NetFPGA router is connects through a single bottleneck link to the server.

We now outline how the various parameters, that are used in the experiments, are varied. Varying the buffer size is straight forward in NetFPGA. The round-trip time can be varied using the Netem tool; this tool allows link delays to be emulated, and thus we can vary the round-trip time. We used the NetFPGA platform's rate limiter

Table 5.1: Parameters used in the NetFPGA experiments

Parameter	*Value*
Buffer size	16, 128 packets
Round-trip time	100 milliseconds
Capacity	946 Mbps
Number of TCP connections	100
Packet size	1500 bytes

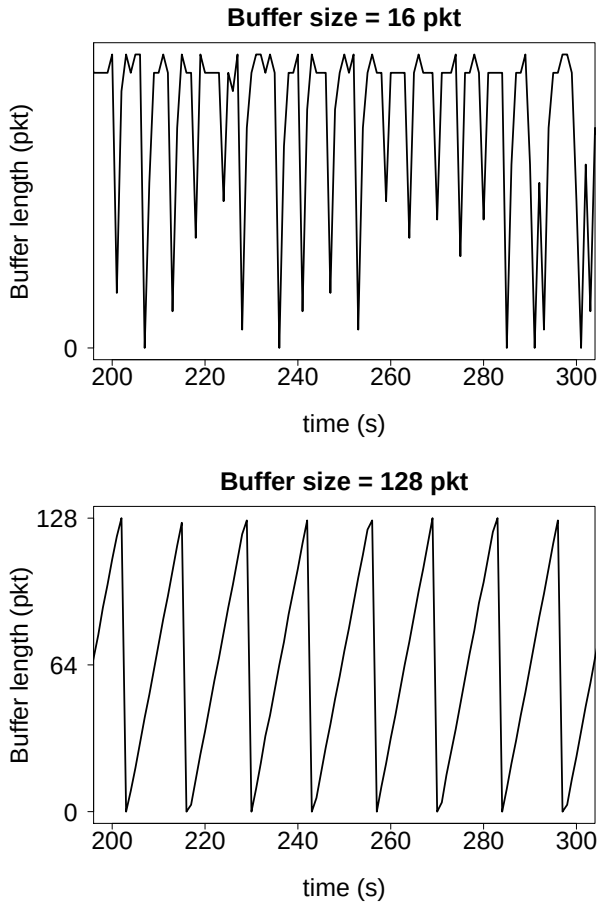

Figure 5.4: With increase in buffer size from 16 to 128, the onset of synchronization with long-lived flows is clearly visible. This confirms the existence of stable limit cycles.

module to limit the data transmission rate on the ethernet port. For generating TCP traffic, and for configuring the number of TCP connections, we used the Iperf tool. The Iperf clients were run on Host 1 and the server was run on Host 2. There is an important difference between the NS2 simulations and the NetFPGA experiments. In

NetFPGA, the data traffic includes packets generated from routing protocol like Open Shortest Path First (OSPF), whereas in the case of NS2 these packets are absent.

The onset of synchronization due to variations in buffer size is observed in Figure 5.4. This constitutes a qualitative change in the dynamics of the system; a phenomena which appears when the buffer size is increased beyond a few dozen packets.

CHAPTER 6

Outlook

In modern communication networks, end-to-end delays associated with processing, queuing, or physical transmission are inherent. Thus delay equations, and their stability and bifurcation analysis, provide a natural setting for understanding some of the aspects of network dynamics.

6.1 Contributions

We conducted a local stability and a detailed Hopf bifurcation analysis of a fluid model for TCP Reno coupled with four queue management policies in network routers. For queue management, we considered the currently implemented Drop-Tail queue policy, in a small and an intermediate buffer regime, and a model for a threshold based queue policy. The Drop-Tail queue policy was investigated in the presence of smooth as well as bursty flows. The local stability analysis, of the various underlying models, allowed us to capture relationships between protocol and queue management parameters to ensure stability. Variations in these parameters, like the router buffer size, was shown to readily induce a Hopf bifurcation. An analytical characterisation of the existence, uniqueness and stability of the bifurcating solutions was conducted using the theory of normal forms and the centre manifold theorem. Practically, stable limit cycles in the queue size can hurt end-to-end performance; and their existence was substantiated via packet-level simulations NetFPGA emulation.

Stability of queues, and low latency, in communication networks are both important metrics for performance evaluation and quality of service. Implementation of the suggested design considerations would ensure both stable queue size dynamics and low latency networks.

6.2 Avenues for further study

The analysis described in the thesis can be extended to queue management strategies such as RED (3) and other TCP congestion avoidance algorithms. A natural extension would be to analyse a multi-bottleneck link as well as a combination of short-lived and long-lived flows in the network. We could also extend the work to other types of TCP like CUBIC (5), which use data loss as the type of feedback signal in the network.

APPENDIX A

Analytical characterisation of Hopf Bifurcation

The structure of this Appendix is as follows: In an autonomous non-linear equation with a single discrete delay we first give conditions for the loss of local stability to occur via a *Hopf bifurcation* (6). Then following the analysis outlined in (6), we perform the necessary calculations to determine the type of the Hopf bifurcation and the asymptotic form of the bifurcating solutions just as local instability sets in.

Consider the non-linear delay-differential equation:

$$\frac{d}{dx}x(t) = \kappa f(x(t), x(t-\tau)), \tag{A.1}$$

where f has a unique equilibrium point denoted by (x^*, y^*) and κ, $\tau > 0$. Define $u(t) = x(t) - x^*$, and take a Taylor expansion of (A.1) including the linear, quadratic, and cubic terms to obtain (4.6). Remember that in (4.6),

$$\xi_{x^i y^j} = \frac{1}{(i+j)!}\frac{\partial^{i+j}}{\partial x^i \partial y^j} f \Big|_{x=x_s, y=y_s}. \tag{A.2}$$

Consider the linearised form of (A.1), namely

$$\frac{d}{dx}x(t) = \kappa\xi_x u(t) + \kappa\xi_y u(t-\tau). \tag{A.3}$$

The stability of (A.3) is given by the roots of the associated characteristic equation.

Theorem 1 *(10) Consider a linear autonomous delay equation whose corresponding characteristic equation is given by* $\lambda + \kappa a + \kappa b e^{-\lambda\tau} = 0$, *where* $\kappa, a, b, \tau > 0$ *and* $b > a$. *Then the trivial solution of the corresponding system is stable for all* $\kappa \in (0, \kappa_c)$ *and undergoes a Hopf bifurcation at* $\kappa = \kappa_c$, *where* $\kappa_c\tau = \frac{\cos^{-1}(-a/b)}{\sqrt{b^2-a^2}}$.

The calculations that follow will enable us to address questions about the form of bifurcating solutions of (A.1) as it transits from stability to instability via a Hopf bifurcation. For this we have to take the quadratic and the cubic terms of (A.1) into consideration. Following the style of analysis in (6), we now perform the requisite calculations.

Consider the autonomous delay-differential system:

$$\frac{d}{dt}u(t) = L_\mu u_t + F(u_t, \mu) \tag{A.4}$$

$t > 0$, $\mu \in R$, where for $\tau > 0$

$$u_t(\theta) = u(t+\theta) \quad u : [-\tau, 0] \in R, \quad \theta \in [-\tau, 0].$$

L_μ is a one parameter family of continuous (bounded) linear operators defined as $L_\mu : C[-\tau, 0] \to R$. The operator $F(u_t, \mu) : C[-\tau, 0] \to R$ contains the non-linear terms. Further, assume that $F(u_t, \mu)$ is analytic and that F and L_μ depends analytically on the *bifurcation parameter* μ for small $|\mu|$. The objective now is to cast (A.4) into the form,

$$\frac{d}{dt}u_t = A(\mu)u_t + Ru_t \tag{A.5}$$

which has u_t rather than both u and u_t. First, transform the linear problem $(d/dt)u(t) = L_\mu u_t$. By the *Riesz representation theorem*, there exists an $n \times n$ matrix valued function $\eta(\theta, \mu) : [-\tau, 0] \to R^{n^2}$, such that each component of η has bounded variation and for all $\phi \in C[-\tau, 0]$

$$L_\mu \phi = \int_{-\tau}^{0} d\eta(\theta, \mu)\phi(\theta).$$

In particular

$$L_\mu u_t = \int_{-\tau}^{0} d\eta(\theta, \mu)u(t+\theta). \tag{A.6}$$

Observe that

$$d\eta(\theta, \mu) = (\kappa\xi_x\delta(\theta) + \kappa\xi_y\delta(\theta+\tau))d\theta,$$

where $\delta(\theta)$ is the Dirac delta function, would satisfy (A.6).

For $\phi \in C^1[-\tau, 0]$, define

$$A(\mu)\phi(\theta) = \begin{cases} \frac{d\phi(\theta)}{d\theta}, & \theta \in [-\tau, 0] \\ \int_{-\tau}^{0} d\eta(s,\mu)\phi(s) \equiv L_\mu \phi, & \theta = 0 \end{cases} \tag{A.7}$$

and

$$R\phi(\theta) = \begin{cases} 0, & \theta \in [-\tau, 0] \\ F(\phi, \mu), & \theta = 0. \end{cases}$$

Then, as $du_t/d\theta \equiv du_t/dt$, system (A.4) becomes (A.5).

The bifurcating periodic solutions $u(t, \mu(\epsilon))$ of (A.4) (where $\epsilon \geq 0$ is a small parameter) have amplitude $O(\epsilon)$, period $P(\epsilon)$, and nonzero Floquet exponent $\beta(\epsilon)$, where μ, P and β have the following (convergent) expansions:

$$\begin{aligned} \mu &= \mu_2\epsilon^2 + \mu_4\epsilon^4 + ... \\ P &= \frac{2\pi}{\omega_0}(1 + T_2\epsilon^2 + T_4\epsilon^4 + ... \\ \beta &= \beta_2\epsilon^2 + \beta_4\epsilon^4 + ... \end{aligned} \tag{A.8}$$

These coefficients will now be determined. Since we only need to compute the expressions at $\mu = 0$, we set $\mu = 0$. Let $q(\theta)$ be the eigenfunction for $A(0)$ corresponding to $\lambda(0)$,

$$A(0)q(\theta) = i\omega_0 q(\theta),$$

and define the adjoint operator $A^*(0)$ as

$$A^*(0)\alpha(s) = \begin{cases} -\frac{d\alpha(s)}{ds}, & s \in (0, \tau] \\ \int_{-\tau}^{0} d\eta^T(t,0)\alpha(-t), & s = 0, \end{cases}$$

where η^T denotes the transpose of η.

The domains of A and A^* are $C^1[-\tau, 0]$ and $C^1[0, \tau]$. As

$$Aq(\theta) = \lambda(0)q(\theta)$$

$\bar{\lambda}(0)$ is an eigenvalue for A^*, and

$$A^*q^* = -i\omega_0 q^*$$

for some nonzero vector q^*. For $\phi \in C[-\tau, 0]$ and $\psi \in C[0, \tau]$ define an inner product

$$\langle \psi, \phi \rangle = \bar{\psi}(0) \cdot \phi(0) - \int_{\theta=-\tau}^{0} \int_{\zeta=0}^{\theta} \bar{\psi}^T(\zeta - \theta) d\eta(\theta) \phi(\zeta) d\zeta, \tag{A.9}$$

where $a \cdot b$ means $\sum_{i=1}^{n} a_i b_i$. Then $\langle \psi, A\phi \rangle = \langle A^*\psi, \phi \rangle$ for $\phi \in \mathrm{Dom}(A)$, $\psi \in \mathrm{Dom}(A^*)$. Let $q(\theta) = e^{i\omega_0\theta}$ and $q^*(s) = De^{i\omega_0 s}$ be the eigenvectors for A and A^* corresponding to the eigenvalues $+i\omega_0$ and $-i\omega_0$. With

$$D = \frac{1}{1 + \tau\kappa\xi_y e^{i\omega_0\tau}},$$

we get $\langle q, q^* \rangle = 1$ and $\langle q^*, \bar{q} \rangle = 0$. Using (A.9), we first confirm $\langle q^*, q \rangle = 1$

$$\begin{aligned} \langle q^*, q \rangle &= \bar{D} - \bar{D}\kappa \int_{\theta=-\tau}^{0} \theta e^{i\omega_0\theta} (\xi_x \delta(\theta) + \xi_y \delta(\theta + \tau)) d\theta \\ &= \bar{D} + \bar{D}\kappa\tau\xi_y e^{-i\omega_0\tau} \\ &= 1. \end{aligned}$$

Similarly we can show that $\langle q^*, \bar{q} \rangle = 0$. Again, using (A.9), we get

$$\begin{aligned} \langle q^*, q \rangle &= \bar{D} + \frac{\bar{D}\kappa}{2i\omega_0} \int_{\theta=-\tau}^{0} \theta (e^{-i\omega_0\theta} - e^{i\omega_0\theta}) (\xi_x \delta(\theta) \\ &\quad + \xi_y \delta(\theta + \tau) d\theta \\ &= \bar{D} + \frac{\bar{D}\kappa}{2i\omega_0} \xi_y (e^{i\omega_0\tau} - e^{-i\omega_0\tau}) \\ &= 0. \end{aligned}$$

For u_t, a solution of (A.5) at $\mu = 0$, define

$$z(t) = \langle q^*, u_t \rangle,$$

and

$$w(t, \theta) = u_t(\theta) - 2\mathrm{Re}\{z(t)q(\theta)\}.$$

Then, on the manifold, C_0, $w(t, \theta) = w(z(t), \bar{z}(t), \theta)$ where

$$w(z, \bar{z}, \theta) = w_{20}(\theta)\frac{z^2}{2} + w_{11}(\theta)z\bar{z} + w_{02}(\theta)\frac{\bar{z}^2}{2} + ... \tag{A.10}$$

In effect, z and $\bar{z}$ are local coordinates for C_0 in C in the directions of q^* and $\bar{q}^*$, respectively. Note that w is real if u_t is real and we deal only with real solutions. The existence of the center manifold C_0 enables us to reduce (A.5) to an ordinary differential equation for a single complex variable on C_0. At $\mu = 0$, this is

$$\begin{aligned} z'(t) &= \langle q^*, Au_t + Ru_t \rangle \\ &= i\omega_0 z(t) + \bar{q}^*(0) \cdot F(w(z, \bar{z}, \theta) + 2\mathrm{Re}\{z(t)q(\theta)\}) \\ &= i\omega_0 z(t) + \bar{q}^*(0) \cdot F_0(z, \bar{z}) \end{aligned} \tag{A.11}$$

which is written in abbreviated form as

$$z'(t) = i\omega_0 z(t) + g(z, \bar{z}). \tag{A.12}$$

Our objective is to expand g in powers of z and $\bar{z}$. We also have to determine the coefficients $w_{ij}(\theta)$ in (A.10). Once the w_{ij} have been determined, the differential equation (A.11) for z would be explicit [as abbreviated in (A.12)] where expanding the function $g(z, \bar{z})$ in powers of z and $\bar{z}$ we have

$$\begin{aligned} g(z, \bar{z}) &= \bar{q}^*(0) \cdot F_0(z, \bar{z}) \\ &= g_{20}\frac{z^2}{2} + g_{11}z\bar{z} + g_{02}\frac{\bar{z}^2}{2} + g_{21}\frac{z^2\bar{z}}{2} + ... \end{aligned}$$

Following (6) we write

$$w' = u_t' - z'q - \bar{z}'\bar{q},$$

and using (A.5) and (A.12) we obtain

$$w' = \begin{cases} Aw - 2\mathrm{Re}\{\bar{q}^*(0) \cdot F_0 q(\theta))\}, & \theta \in [-\tau, 0) \\ Aw - 2\mathrm{Re}\{\bar{q}^*(0) \cdot F_0 q(0))\} + F_0, & \theta = 0, \end{cases}$$

which is rewritten as

$$w' = Aw + H(z, \bar{z}, \theta) \tag{A.13}$$

using (A.10), where

$$H(z, \bar{z}, \theta) = H_{20}(\theta)\frac{z^2}{2} + H_{11}(\theta)z\bar{z} + H_{02}(\theta)\frac{\bar{z}^2}{2} + ... \tag{A.14}$$

Now, on C_0, near the origin

$$w' = w_z z' + w_{\bar{z}}\bar{z}'.$$

Using (A.10) and (A.12) to replace w_z, z' (and their conjugates by their power series expansion) and equating this with (A.13), we get (6)

$$\begin{aligned} (2i\omega_0 - A)w_{20}(\theta) &= H_{20}(\theta) \\ -Aw_{11}(\theta) &= H_{11}(\theta) \\ -(2i\omega_0 + A)w_{02}(\theta) &= H_{02}(\theta). \end{aligned}$$

We start by observing

$$\begin{aligned} u_t(\theta) &= w(z, \bar{z}, \theta) + zq(\theta) + \bar{z}\bar{q}(\theta) \\ &= w_{20}(\theta)\frac{z^2}{2} + w_{11}(\theta)z\bar{z} + w_{02}(\theta)\frac{\bar{z}^2}{2} \\ &+ ze^{i\omega_0\theta} + \bar{z}e^{-i\omega_0\theta} + ... \end{aligned}$$

from which we obtain $u_t(0)$ and $u_t(-\tau)$. We have actually looked ahead, and as we will only be requiring the coefficients of z^2, $z\bar{z}$, $\bar{z}^2$, and $z^2\bar{z}$, we only keep these relevant

terms in the following expansions:

$$
\begin{aligned}
u_t^2(0) &= (w(z,\bar{z},0)+z+\bar{z})^2 \\
&= z^2+\bar{z}^2+2z\bar{z} \\
&+z^2\bar{z}(2w_{11}(0)+w_{20}(0))+... \\
u_t(0)u_t(-\tau) &= (w(z,\bar{z},0)+z+\bar{z}) \\
&\times(w(z,\bar{z},-\tau)+ze^{-i\omega_0\tau}+\bar{z}e^{i\omega_0\tau}) \\
&= z^2e^{-i\omega_0\tau}+z\bar{z}(e^{i\omega_0\tau} \\
&+e^{-i\omega_0\tau})+\bar{z}^2e^{i\omega_0\tau} \\
&+z^2\bar{z}\left(w_{11}(0)e^{-i\omega_0\tau}+\frac{w_{20}(0)}{2}e^{i\omega_0\tau}\right. \\
&\left.+w_{11}(-\tau)+\frac{w_{20}(-\tau)}{2}\right)+... \\
\\
u_t^2(-\tau) &= (w(z,\bar{z},-\tau)+ze^{-i\omega_0\tau}+\bar{z}e^{i\omega_0\tau})^2 \\
&= z^2e^{-2i\omega_0\tau}+\bar{z}^2e^{2i\omega_0\tau}+2z\bar{z} \\
&+z^2\bar{z}(2e^{-i\omega_0\tau}w_{11}(-\tau) \\
&+e^{i\omega_0\tau}w_{20}(-\tau))+... \\
u_t^3(0) &= (w(z,\bar{z},0)+z+\bar{z})^3 \\
&= 3z^2\bar{z}+... \\
u_t^2(-\tau)u_t(0) &= (w(z,\bar{z},-\tau)+ze^{-i\omega_0\tau}+\bar{z}e^{i\omega_0\tau})^2 \\
&\times(w(z,\bar{z},0)+z+\bar{z}) \\
&= z^2\bar{z}(e^{-2i\omega_0\tau}+2)+... \\
u_t^2(0)u_t(-\tau) &= (w(z,\bar{z},0)+z+\bar{z})^2 \\
&\times(w(z,\bar{z},-\tau)+ze^{-i\omega_0\tau}+\bar{z}e^{i\omega_0\tau}) \\
&= z^2\bar{z}(e^{i\omega_0\tau}+2e^{-i\omega_0\tau})+... \\
u_t^3(-\tau) &= (w(z,\bar{z},-\tau)+ze^{-i\omega_0\tau}+\bar{z}e^{i\omega_0\tau})^3 \\
&= 3z^2\bar{z}e^{-i\omega_0\tau}+...
\end{aligned}
$$

Recall that

$$
\begin{aligned}
g(z,\bar{z}) &= \bar{q}^* \cdot F_0(z,\bar{z}) \ \text{ and} \\
g(z,\bar{z}) &= g_{20}\frac{z^2}{2} + g_{11}z\bar{z} + g_{02}\frac{\bar{z}^2}{2} + g_{21}\frac{z^2\bar{z}}{2} + ...
\end{aligned}
$$

After collecting the coefficients of z^2, $z\bar{z}$, $\bar{z}^2$, and $z^2\bar{z}$, we are in a position to calculate the coefficients of g_{20}, g_{11}, g_{01}, and g_{21}, which are

$$g_{20} = \bar{q}^*(0)\kappa[2\xi_{xx} + 2\xi_{xy}e^{-i\omega_0\tau} + 2\xi_{yy}e^{-2i\omega_0\tau}] \tag{A.15}$$

$$g_{11} = \bar{q}^*(0)\kappa[2\xi_{xx} + 2\xi_{xy}(e^{i\omega_0\tau} + e^{-i\omega_0\tau}) + 2\xi_{yy}] \tag{A.16}$$

$$g_{02} = \bar{q}^*(0)\kappa[2\xi_{xx} + 2\xi_{xy}e^{i\omega_0\tau} + 2\xi_{yy}e^{2i\omega_0\tau}] \tag{A.17}$$

$$
\begin{aligned}
g_{21} = \bar{q}^*(0)\kappa[&2\xi_{xx}(2w_{11}(0) + w_{20}(0)) \\
&+ \xi_{xy}(2w_{11}(0)e^{-i\omega_0\tau} + w_{20}(0)e^{i\omega_0\tau} \\
&+ 2w_{11}(-\tau) + 2w_{20}(-\tau)) \\
&+ \xi_{yy}(4w_{11}(-\tau))e^{-i\omega_0\tau} + 2w_{20}(-\tau)e^{i\omega_0\tau}) \\
&+ 6\xi_{xxx} + \xi_{xyy}(2e^{-2i\omega_0\tau} + 4) \\
&+ \xi_{xxy}(2e^{i\omega_0\tau} + 4e^{-i\omega_0\tau}) + 6\xi_{yyy}e^{-i\omega_0\tau}].
\end{aligned} \tag{A.18}
$$

Observe that in the expression for g_{21} we have $w_{11}(0)$, $w_{11}(-\tau)$, $w_{20}(0)$, and $w_{20}(-\tau)$ which we still need to evaluate. Now, for $\theta \in [-\tau, 0]$

$$
\begin{aligned}
H(z,\bar{z},\theta) &= -2\mathrm{Re}\{\bar{q}^*(0) \cdot \ F_0 q(\theta)\} \\
&= -2\mathrm{Re}\{g(z,\bar{z})q(\theta)\} \\
&= -g(z,\bar{z})q(\theta) - \bar{g}(z,\bar{z})\bar{q}(\theta) \\
&= -\left(g_{20}\frac{z^2}{2} + g_{11}z\bar{z} + g_{02}\frac{\bar{z}^2}{2} + ...\right)q(\theta) \\
&\quad -\left(\bar{g}_{20}\frac{\bar{z}^2}{2} + \bar{g}_{11}z\bar{z} + \bar{g}_{02}\frac{z^2}{2} + ...\right)\bar{q}(\theta),
\end{aligned} \tag{A.19}
$$

which when compared with (A.14) yields,

$$
\begin{aligned}
H_{20}(\theta) &= -g_{20}q(\theta) - \bar{g}_{02}\bar{q}(\theta) \\
H_{11}(\theta) &= -g_{11}q(\theta) - \bar{g}_{11}\bar{q}(\theta).
\end{aligned}
$$

We already noted that,

$$(2i\omega_0 - A)w_{20}(\theta) = H_{20}(\theta) \tag{A.20}$$

$$-Aw_{11}(\theta) = H_{11}(\theta) \tag{A.21}$$

$$-(2i\omega_0 + A)w_{02}(\theta) = H_{02}(\theta). \tag{A.22}$$

From (A.7), (A.20), (A.21) we get the following equations:

$$w'_{20}(\theta) = 2i\omega_0 w_{20}(\theta) + g_{20}q(\theta) + \bar{g}_{02}\bar{q}(\theta) \tag{A.23}$$

$$w'_{11}(\theta) = g_{11}q(\theta) + \bar{g}_{11}\bar{q}(\theta). \tag{A.24}$$

Solving the differential equations (A.23) and (A.24) gives us

$$w_{20}(\theta) = -\frac{g_{20}}{i\omega_0}q(0)e^{i\omega_0\theta} - \frac{\bar{g}_{02}}{3i\omega_0}\bar{q}(0)e^{-i\omega_0\theta} + Ee^{2i\omega_0\theta} \tag{A.25}$$

$$w_{11}(\theta) = \frac{g_{11}}{i\omega_0}q(0)e^{i\omega_0\theta} - \frac{\bar{g}_{11}}{i\omega_0}\bar{q}(0)e^{-i\omega_0\theta} + F \tag{A.26}$$

for some E, F which will soon be determined. Now, for $H(z, \bar{z}, 0) = -2\mathrm{Re}(\bar{q}^*(0)) \cdot F_0q(0)) + F_0$,

$$\begin{aligned} H_{20}(0) &= -g_{20}q(0) - \bar{g}_{02}\bar{q}(0) \\ &\quad + \kappa(2\xi_{xx} + 2\xi_{xy}e^{-i\omega_0\tau} + 2\xi_{yy}e^{-2i\omega_0\tau}) \end{aligned} \tag{A.27}$$

$$\begin{aligned} H_{11}(0) &= -g_{11}q(0) - \bar{g}_{11}\bar{q}(0) \\ &\quad + \kappa(2\xi_{xx} + \xi_{xy}(e^{i\omega_0\tau} + e^{-i\omega_0\tau}) + 2\xi_{yy}). \end{aligned} \tag{A.28}$$

From (A.7), (A.20), (A.21), we get

$$\begin{aligned} &\kappa\xi_x w_{20}(0) + \kappa\xi_y w_{20}(-\tau) - 2i\omega_0 w_{20}(0) \\ &\qquad = g_{20}q(0) + \bar{g}_{02}\bar{q}(0) \\ &\qquad - \kappa(2\xi_{xx} + 2\xi_{xy}e^{-i\omega_0\tau} + 2\xi_{yy}e^{-2i\omega_0\tau}) \end{aligned} \tag{A.29}$$

$$\begin{aligned}
&\kappa\xi_x w_{11}(0) + \kappa\xi_y w_{11}(-\tau) \\
&\qquad = g_{11}q(0) + \bar{g}_{11}\bar{q}(0) \\
&\qquad - \kappa(2\xi_{xx} + \xi_{xy}(e^{i\omega_0\tau} + e^{-i\omega_0\tau}) + 2\xi_{yy}).
\end{aligned} \tag{A.30}$$

We have the solution for $w_{20}(\theta)$ and $w_{11}(\theta)$ from (A.25) and (A.26), respectively. Hence, evaluate $w_{20}(0)$, $w_{20}(-\tau)$, $w_{11}(0)$, and $w_{11}(-\tau)$, substitute in (A.29) and (A.30), respectively, and calculate E, F as

$$\begin{aligned}
E &= \frac{\phi_1}{\kappa\xi_x + \kappa\xi_y e^{-2i\omega_0\tau} - 2i\omega_0} \\
F &= \frac{\phi_2}{\kappa\xi_x + \kappa\xi_y}
\end{aligned}$$

where

$$\begin{aligned}
\phi_1 &= (\kappa\xi_x - 2i\omega_0)\left(\frac{g_{20}}{i\omega_0} + \frac{\bar{g}_{02}}{3i\omega_0}\right) \\
&\quad + \kappa\xi_y\left(\frac{g_{20}}{i\omega_0}e^{-i\omega_0\tau} + \frac{\bar{g}_{02}}{3i\omega_0}e^{i\omega_0\tau}\right) + \text{RHS of (A.29)} \\
\phi_2 &= -(\kappa\xi_x)\left(\frac{g_{11}}{i\omega_0} - \frac{\bar{g}_{11}}{i\omega_0}\right) \\
&\quad - \kappa\xi_y\left(\frac{g_{11}}{i\omega_0}e^{-i\omega_0\tau} - \frac{\bar{g}_{11}}{3i\omega_0}e^{i\omega_0\tau}\right) \\
&\quad + \text{RHS of (A.30)}.
\end{aligned}$$

All the quantities required for the computations associated for the stability analysis of the Hopf bifurcation are completed. The analysis can be performed using

$$c_1(0) = \frac{i}{2\omega_0}\left(g_{20}g_{11} - 2|g_{11}|^2 - \frac{1}{3}|g_{02}|^2\right) + \frac{g_{21}}{2} \tag{A.31}$$

$$\mu_2 = \frac{-\mathrm{Re}c_1(0)}{\alpha'(0)} \tag{A.32}$$

$$P = \frac{2\pi}{\omega_0}(1 + \epsilon^2 T_2 + O(\epsilon^4)) \tag{A.33}$$

$$T_2 = -\left(\frac{\mathrm{Im}c_1(0) + \mu_2\omega'(0)}{\omega_0}\right) \tag{A.34}$$

$$\beta = \epsilon^2\beta_2 + O(\epsilon^4) \;\; \beta_2 = 2\mathrm{Re}c_1(0) \;\; \epsilon = \sqrt{\frac{\mu}{\mu_2}}, \tag{A.35}$$

where $c_1(0)$ is the lyapunov coefficient and g_{20}, g_{11}, g_{02}, g_{21} are defined by (A.15)-(A.18), respectively.

To use κ to induce instability let $\kappa = \kappa_c + \mu$, where a Hopf bifurcation takes place at $\mu = 0$, where κ_c may evaluated from theorem 1. Then $\alpha'(0)$ and $\omega'(0)$ are the real and imaginary components of $(d\lambda/d\kappa)$ evaluated at $\kappa = \kappa_c$.

We now state the conditions that will enable us to verify the stability of the Hopf bifurcation.

- The sign of μ_2 determines the direction of bifurcation. If $\mu_2 > 0$ then the Hopf bifurcation is *supercritical* and if $\mu_2 < 0$ it is *subcritical*.
- The sign of (the Floquet exponent) β_2 determines the stability of the bifurcating periodic solutions. The periodic solutions are *asymptotically orbitally stable* if $\beta_2 < 0$ and unstable if $\beta_2 > 0$.

REFERENCES

[1] P. Costa, A. Donnelly, A. Rowstron and G. O'Shea, "Camdoop: Exploiting in-network aggregation for big data applications", in *Proceedings of USENIX NSDO*, 2012.

[2] G. Covington, G. Adam, G. Gibb, J.W. Lockwood and N. McKeown, "A packet generator on the NetFPGA platform", in *Proceedings of IEEE Symposium on FCCM*, 2009.

[3] S. Floyd and V. Jacobson, "Random early detection gateways for congestion avoidance", *ACM/IEEE Transactions on Networking*, vol. 1, pp. 397–413, 1993.

[4] G. Gibb, J.W. Lockwood, J. Naous, P. Hartke and N. McKeown, "NetFPGA–An open platform for teaching how to build gigabit-rate network switches and routers", *IEEE Transactions on Education*, vol. 51, pp. 364–369, 2008.

[5] S. Ha, I. Rhee and L. Xu, "CUBIC: a new TCP-friendly high-speed TCP variant", *ACM SIGOPS Operating Systems Review*, vol. 42, pp. 64–74, 2008.

[6] B.D. Hassard, N.D. Kazarinoff and Y.H. Wan, *Theory and applications of Hopf bifurcation*, Cambridge University Press, 1981.

[7] F.P. Kelly, "Models for a self-managed Internet", *Philosophical Transactions of the Royal Society*, vol. 358, pp. 2335–2348, 2000.

[8] S. Kunniyur and R. Srikant, "End-to-end congestion control schemes: utility functions, random losses and ECN marks", *ACM/IEEE Transactions on Networking*, vol. 11, pp. 689–702, 2003.

[9] V. Misra, W.B. Gong and D. Towsley, "Fluid-based analysis of a network of AQM

routers supporting TCP flows with an application to RED", in *Proceedings of ACM/SIGCOMM*, 2000.

[10] G. Raina, "Local bifurcation analysis of some dual congestion control algorithms", *IEEE Transactions on Automatic Control*, vol. 50, pp. 1135–1146, 2005.

[11] G. Raina, D. Towsley and D. Wischik, "Part II: Control theory for buffer sizing", *ACM/SIGCOMM Computer Communication Review*, vol. 35, pp. 79–82, 2005.

[12] G. Raina and D. Wischik, "Buffer sizes for large multiplexers: TCP queueing theory and instability analysis", in *Proceedings of Next Generation Internet Networks*, 2005.

[13] D. Wischik, "Buffer sizing theory for bursty TCP flows", in *Proceedings of International Zurich Seminar Communications*, 2006.

[14] G. Vinnicombe, *Uncertainty and Feedback: $\mathscr{H}_\infty$ loop-shaping and the ν-gap metric*, World Scientific, 2001.

[15] D. Wischik and N. McKeown, "Part I: Buffer sizes for core routers", *ACM SIGCOMM Computer Communication Review*, vol. 35, pp. 75–78, 2005.

[16] The Network Simulator (NS2). [Online]. Available: `http://nsnam.isi.edu/nsnam/index.php/UserInformation`.

LIST OF PAPERS BASED ON THESIS

1. A. Mohan, S. Raman and G. Raina,“TCP Reno and queue management: local stability and Hopf bifurcation analysis", *Submitted to the 52nd IEEE Conference on Decision and Control*, 2013.